Fermi National Accelerator Laboratory

FERMILAB-FN-604

Longitudinal Emittance Increase due to Sinusoidal Perturbation

King-Yuen Ng

Fermi National Accelerator Laboratory
P.O. Box 500, Batavia, Illinois 60510

June 1993

Operated by Universities Research Association Inc. under Contract No. DE-AC02-76CHO3000 with the United States Department of Energy

Disclaimer

FN-604

LONGITUDINAL EMITTANCE INCREASE DUE TO SINUSOIDAL PERTURBATION

King-Yuen Ng

Fermi National Accelerator Laboratory, P.O. Box 500, Batavia, IL 60510*

(June 1993)

---

*Operated by the Universities Research Association, Inc., under contract with the U.S. Department of Energy.

I. INTRODUCTION

In a previous paper [1], the longitudinal motion of a particle under periodic ground motion perturbation was studied with the assumption of no spread in the synchrotron frequency. It was shown that the rf phase mismatch due to sinusoidal ground-wave kick on the quadrupoles does not add up so as to throw the particle outside the rf bucket, except in the unlikely event that the discrete driving frequency of the perturbation is locked on exactly at the synchrotron frequency. The rf force is nonlinear, which reduces the synchrotron frequency to zero at the boundary of the rf bucket. As a result, the response due to a perturbation of any frequency will not kick the particle into resonance. However, the nonlinear rf force does introduce resonances of another sort: the existence of islands in the longitudinal phase space. The motion of beam particles inside these islands will lead to an increase in the longitudinal emittance of the particle bunch.

II. EQUATIONS OF MOTION

Consider a beam particle in an accelerator ring with its orbit subject to a horizontal bend $\theta(t) = \hat{\theta}\sin\omega_m t$, where $\omega_m/2\pi$ is the driving frequency. This sinusoidal bend can arise from the horizontal ground-motion wave pounding on the quadrupoles, or the power ripple of a current bus on the dipoles. If the lattice has a dispersion D at the point of perturbation, the length of the closed orbit C will 1experience a fluctuation [1]

$$\Delta C = D\theta(t) \; . \tag{2.1}$$

The rf phase offset φ and energy offset δ of the beam particle at the $(n+1)$th turn are given by

$$\begin{aligned} \varphi_{n+1} &= \varphi_n \pm \frac{2\pi h|\eta|}{\beta^2}\delta_n + 2\pi h\frac{\Delta C}{C} \; , \\ \delta_{n+1} &= \delta_n \mp \frac{eV}{E}\sin\varphi_{n+1} \; , \end{aligned} \tag{2.2}$$

where h is the rf harmonic, η is the phase-slip parameter, E and βc are the energy and velocity of the synchronous particle, and c is the velocity of light. The particle is assumed in a stationary bucket with rf voltage V. The upper (lower) signs apply when the energy of the particle is above (below) transition. Since the synchrotron tune at zero amplitude

$$\nu_{s0} = \sqrt{\frac{|\eta|heV}{2\pi\beta^2 E}} \tag{2.3}$$

is usually much less than unity, the discrete equations of motion can be approximated by differential equations:

$$\frac{d\varphi}{d\theta} = \nu_{s0}\delta + a\nu_{s0}\sin\nu_m\theta \ ,$$

$$\frac{d\delta}{d\theta} = -\nu_{s0}\sin\varphi \ , \tag{2.4}$$

where δ has been rescaled

$$\delta \to \sqrt{\frac{eV\beta^2}{2\pi|\eta|h}}\,\delta \tag{2.5}$$

so that the two equations appear to be more symmetric. In the above, the situation of above transition has been chosen, $\nu_m = \omega_m/\omega_0$ is the tune of the perturbation, and $\omega_0/2\pi$ is the revolution frequency. The independent variable θ denotes the azimuthal angle around the accelerator ring; it advances by 2π for every turn. We have introduced a dimensionless parameter

$$a = \frac{hD\hat{\theta}}{\nu_{s0}} \tag{2.6}$$

to denote the amplitude of the driving perturbation. These equations of motion can be derived conveniently from the Hamiltonian

$$H = \tfrac{1}{2}\nu_{s0}\delta^2 + \nu_{s0}(1-\cos\varphi) + a\delta\nu_{s0}\sin\nu_m\theta \ . \tag{2.7}$$

III. HAMILTONIAN

The unperturbed Hamiltonian (with $a = 0$) is exactly that of a pendulum and can be solved exactly. The ground motion or current ripple can then be treated as a perturbation.

In the absence of the perturbation, the unperturbed Hamiltonian can be written as

$$H_0 = \tfrac{1}{2}\nu_{s0}\delta^2 + \nu_{s0}(1 - \cos\varphi) = 2\nu_{s0}k^2 \ , \tag{3.1}$$

where

$$k = \sin\tfrac{1}{2}\varphi_0 \ , \tag{3.2}$$

and φ_0 is the maximum oscillation amplitude of the pendulum. Define a new variable z by

$$\sin\tfrac{1}{2}\varphi = k\sin z \ , \tag{3.3}$$

where z reaches π as the amplitude swings to $\varphi = \varphi_0$.

The action J is defined as

$$J = \frac{1}{2\pi}\oint \delta d\varphi \ , \tag{3.4}$$

where

$$\delta = 2k\sqrt{1 - k^{-2}\sin^2\tfrac{\varphi}{2}} \ . \tag{3.5}$$

is obtained from Eq. (3.1).

Since

$$\cos\tfrac{1}{2}\varphi = \sqrt{1-k^2\sin^2 z} \qquad \text{and} \qquad \tfrac{1}{2}\cos\tfrac{1}{2}\varphi\, d\varphi = k\cos z\, dz\ , \tag{3.6}$$

we get

$$J = \frac{8}{\pi}\int_0^{\frac{\pi}{2}} \frac{k^2\cos^2 z}{\sqrt{1-k^2\sin^2 z}}\, dz = \frac{8}{\pi}\left[E(k) - (1-k^2)K(k)\right]\ , \tag{3.7}$$

where $K(k)$ and $E(k)$ are complete elliptical integrals of the first and second kinds. One of the equations of motion is

$$\frac{d\varphi}{d\theta} = \nu_{s0}\delta = 2k\nu_{s0}\cos z\ . \tag{3.8}$$

After rearranging and changing variable from φ to z, we obtain

$$\nu_{s0}\theta = \int_0^z \frac{dz}{\sqrt{1-k^2\sin^2 z}}\ . \tag{3.9}$$

This means that we have

$$\begin{aligned} \mathrm{sn}(\nu_{s0}\theta|k) &= \sin z = k^{-1}\sin\tfrac{\varphi}{2}, \\ \mathrm{cn}(\nu_{s0}\theta|k) &= \cos z\ , \end{aligned} \tag{3.10}$$

where sn and cn are Jacobian elliptic functions. Then, the transformation becomes

$$\begin{aligned} \varphi &= 2\sin^{-1}[k\,\mathrm{sn}(\nu_{s0}\theta|k)]\ , \\ \delta &= 2k\,\mathrm{cn}(\nu_{s0}\theta|k)\ , \end{aligned} \tag{3.11}$$

and the parameter k is given by Eq. (3.2) and is a function of J.

If Eq. (3.9) is integrated from 0 to the maximum amplitude φ_0 (or $z = \frac{1}{2}\pi$), we obtain the pendulum tune $\nu_s(J)$ for finite action J:

$$\frac{2\pi\nu_{s0}}{4\nu_s(J)} = \int_0^{\frac{\pi}{2}} \frac{dz}{\sqrt{1-k^2\sin^2 z}} = K(k)\ , \tag{3.12}$$

or

$$\nu_s(J) = \frac{\pi \nu_{s0}}{2K(k)} \ . \tag{3.13}$$

According to the definition of the action J in Eq. (3.4), the angle variable ψ is given by

$$\psi = \nu_s(J)\theta - \frac{\pi}{2} \ , \tag{3.14}$$

where the constant $-\frac{\pi}{2}$ has been chosen for the sake of convenience. In terms of action-angle variables, the total Hamiltonian can now be rewritten as

$$H = \int_0^J \nu_s(J) dJ + 2ak\nu_{s0} \, \mathrm{cn}(u|k) \sin \nu_m \theta \ , \tag{3.15}$$

where $u = \left(\psi + \frac{\pi}{2}\right) \nu_{s0}/\nu_s(J)$.

With the aid of the expansion formula

$$\mathrm{cn}(u|k) = -\frac{2\pi}{kK(k)} \sum_{n=0}^{\infty} \frac{(-1)^n q^{n+1/2}}{1+q^{2n+1}} \sin(2n+1)\psi \ , \tag{3.16}$$

where the "nome" is defined by

$$q = e^{-\pi K(\sqrt{1-k^2})/K(k)} \ , \tag{3.17}$$

we can see clearly that the perturbing part of the Hamiltonian is a superposition of terms containing

$$\cos[(n+\tfrac{1}{2})\psi \pm \nu_m \theta] \ , \tag{3.18}$$

with $n = 0, \ 1, \ 2, \ \cdots$, implying that there are resonances whenever

$$(2n+1)\nu_s(J) = \nu_m \ . \tag{3.19}$$

These resonances are different from those that occur in the transverse phase space. The island structure rotates with frequency $\omega_m/2\pi$ about the center of the longitudinal phase space. In other words, the island structure only reveals itself when the position of the particle is mapped every perturbation period or $[\nu_m^{-1}]$ turns, where $[\nu_m^{-1}]$ is the integer closest to ν_m^{-1}. This is also evident from the equations of motion, because the right sides of Eq. (2.4) become "time" independent in the ν_m^{-1}-turn map.

IV. FIRST-ORDER RESONANCE

So far the treatment of the Hamiltonian has been exact. To pursue the problem further analytically, however, we need to resort to approximation. We can expand in terms of k which is always less than unity except when the particle is at the boundary of the bucket. Thus,

$$q = \frac{k^2}{16} + 8\left(\frac{k^2}{16}\right)^2 + 84\left(\frac{k^2}{16}\right)^3 + 992\left(\frac{k^2}{16}\right)^4 + \cdots , \tag{4.1}$$

$$K(k) = \frac{\pi}{2}\left[1 + \left(\frac{1}{2}\right)^2 k^2 + \left(\frac{1\cdot 3}{2\cdot 4}\right)^2 k^4 + \left(\frac{1\cdot 3\cdot 5}{2\cdot 4\cdot 6}\right)^2 k^6 + \cdots\right] , \tag{4.2}$$

$$E(k) = \frac{\pi}{2}\left[1 - \left(\frac{1}{2}\right)^2 \frac{k^2}{1} - \left(\frac{1\cdot 3}{2\cdot 4}\right)^2 \frac{k^4}{3} - \left(\frac{1\cdot 3\cdot 5}{2\cdot 4\cdot 6}\right)^2 \frac{k^6}{5} - \cdots\right] . \tag{4.3}$$

We then obtain from Eq. (3.7),

$$k = \sqrt{\frac{J}{2}}\left(1 - \frac{J}{16} + \cdots\right) . \tag{4.4}$$

and the Hamiltonian now becomes

$$H = \nu_{s0}\left(J - \frac{J^2}{16}\right) - a\nu_{s0}\left[(2J)^{1/2}\sin\psi - \frac{(2J)^{3/2}}{64}\sin 3\psi + \cdots\right]\sin\nu_m\theta , \tag{4.5}$$

where only the lowest order of $\sqrt{2J}$ for every harmonic of ψ has been retained.

Although $\sqrt{2J} \to \frac{4}{\sqrt{\pi}}$ when $k \to 1$, the Hamiltonian in Eq. (4.5) is in fact an expansion in k^2, as is indicated in the expansions of cn and q in Eqs. (3.16) and (4.1). Therefore, the higher-order resonances are only important when the oscillation amplitude φ_0 becomes large. For this reason, we are going to concentrate on the first-order resonance here. The relevant parts of the Hamiltonian are:

$$H = \nu_{s0}\left(J - \frac{J^2}{16}\right) - \frac{a\nu_{s0}}{2}(2J)^{1/2}\cos(\psi - \nu_m\theta) . \tag{4.6}$$

We go to a frame rotating with frequency $\omega_m/2\pi$ through the canonical transformation whose generating function is

$$F_2(\hat{J},\psi) = \hat{J}(\psi - \nu_m\theta) \ , \tag{4.7}$$

from which we obtain

$$J = \hat{J} \qquad \text{and} \qquad \hat{\psi} = \psi - \nu_m\theta \ . \tag{4.8}$$

The new Hamiltonian

$$\frac{H}{\nu_{s0}} = xJ - \frac{J^2}{16} - \frac{a}{2}\cos\psi \ , \tag{4.9}$$

becomes "time" independent. For the sake of convenience, we have defined

$$x = 1 - \frac{\nu_m}{\nu_{s0}} \tag{4.10}$$

to take care of the driving frequency ν_m and removed the "hats" from the action-angle variables. The fixed points are given by

$$\begin{aligned} \frac{dJ}{d\theta} &= -\frac{1}{2}a\nu_{s0}\sqrt{2J}\sin\psi = 0 \ , \\ \frac{d\psi}{d\theta} &= \nu_{s0}\left[x - \frac{J}{8} - \frac{a}{2\sqrt{2J}}\cos\psi\right] = 0 \ . \end{aligned} \tag{4.11}$$

We always choose the convention of $\psi = 0$ and allow the phase amplitude $g = \sqrt{2J}$ to attain negative values. Then the equation for the fixed points becomes

$$xg - \frac{g^3}{16} - \frac{a}{2} = 0 \ . \tag{4.12}$$

In general, there are 3 real solutions; but there is only one when x is small enough. The critical point is called the bifurcation point and is given by $dx/dg = 0$, from which the bifurcation frequency and amplitude are found to be

$$x_{bf} = \frac{3}{16}(4a)^{2/3} \qquad \text{and} \qquad g_{bf} = (4a)^{1/3} \ . \tag{4.13}$$

To simplify the derivation, we *normalize* the variables with respect to their bifurcation values:

$$\frac{x}{x_{bf}} \to \hat{x} \qquad \text{and} \qquad \frac{g}{g_{bf}} \to \hat{g} \ , \tag{4.14}$$

thus scaling away the driving amplitude a, so that the equation for fixed points

$$\hat{g}^3 - 3\hat{x}\hat{g} + 2 = 0 \ , \tag{4.15}$$

depends on the variable $\hat{x}$ only. When the driving frequency is below bifurcation ($\hat{x} > 1$), the solutions can be readily written as [2]

$$\begin{aligned}
\hat{g}_a(\hat{x}) &= -\frac{8}{\sqrt{3}}\hat{x}^{1/2}\cos\frac{\xi}{3} \ , \\
\hat{g}_b(\hat{x}) &= \frac{8}{\sqrt{3}}\hat{x}^{1/2}\sin\left(\frac{\pi}{6} - \frac{\xi}{3}\right) \ , \\
\hat{g}_c(\hat{x}) &= \frac{8}{\sqrt{3}}\hat{x}^{1/2}\sin\left(\frac{\pi}{6} + \frac{\xi}{3}\right) \ ,
\end{aligned} \tag{4.16}$$

where $\xi = \tan^{-1}\sqrt{\hat{x}^3 - 1}$. Above bifurcation ($\hat{x} < 1$), the only real solution is

$$\hat{g}_a(\hat{x}) = -\frac{8}{\sqrt{3}}\hat{x}^{1/2}\cosh\frac{\xi}{3} \ , \tag{4.17}$$

where $\xi = \tanh^{-1}\sqrt{1 - \hat{x}^3}$. It is not hard to find by expanding the Hamiltonian around the fixed points that $\hat{g}_a$ and $\hat{g}_b$ are stable fixed points while $\hat{g}_c$ is an unstable fixed point. At bifurcation ($\hat{x} = 1$), Eq. (4.15) becomes

$$(\hat{g} - 1)^2(\hat{g} + 2) = 0 \ , \tag{4.18}$$

implying that $\hat{g}_a = -2$ while $\hat{g}_b$ and $\hat{g}_c$ merge together to 1.

The locations of the fixed points together with the separatrices in the longitudinal phase space are shown in Fig. 1 when the perturbing frequency is below and right at bifurcation.

V. SEPARATRICES

As shown in Fig. 1(a), the separatrices cut the phase axis at points 1, 2, and the unstable fixed point c. Bunch particles near point 2 will be driven to point 1 and c, thus increasing the area of the bunch. It is therefore desired to evaluate the amplitudes $\hat{g}_1$ and $\hat{g}_2$. 220z Since the separatrices pass through the unstable fixed point, their equations are given by equating the Hamiltonian to its value at point c. Again, using the convention of $\psi = 0$, $\hat{g}_1$ and $\hat{g}_2$ satisfy

$$6\hat{x}\hat{g}^2 - \hat{g}^4 - 8\hat{g} = 6\hat{x}\hat{g}_c^2 - \hat{g}_c^4 - 8\hat{g}_c \ . \tag{5.1}$$

This is a quartic with only 3 real roots; therefore $\hat{g}_c$ must be a double root. Since the unstable fixed point $\hat{g}_c$ satisfies

$$\hat{g}_c^3 - 3\hat{x}\hat{g}_c + 2 = 0 \ , \tag{5.2}$$

we can eliminate $\hat{x}$. Then it is simple to factor out $(\hat{g}-\hat{g}_c)^2$, leaving behind a quadratic

$$\hat{g}^2 + 2\hat{g}_c\hat{g} + \hat{g}_c^2 - \frac{4}{\hat{g}_c} = 0 \ . \tag{5.3}$$

The final solution is

$$\begin{aligned} \hat{g}_1 &= -\hat{g}_c - \frac{2}{\sqrt{\hat{g}_c}} \ , \\ \hat{g}_2 &= -\hat{g}_c + \frac{2}{\sqrt{\hat{g}_c}} \ , \end{aligned} \tag{5.4}$$

If point 2 happens to be at the origin, the bunch will be unstable no matter how small it is and will be diverted to point 1 following the separatrices. This occurs when

$$\hat{g}_c = 2^{2/3} \qquad \text{and} \qquad \hat{x} = 2^{1/3} \ , \tag{5.5}$$

where Eqs. (5.2) and (5.4) have been used. At this moment, the maximum phase excursion is

$$\hat{g}_1 = 2^{5/3} . \tag{5.6}$$

The fixed points $\hat{g}_a$, $\hat{g}_b$, and $\hat{g}_c$ as well as the separatrix intercepts $\hat{g}_1$ and $\hat{g}_2$ are plotted in Fig. 2 as functions of the normalized frequency $\hat{x}$.

VI. EMITTANCE INCREASE

Below bifurcation, when the initial normalized phase extent of the bunch $\hat{g}_i$ is larger than $|\hat{g}_1|$, it is clear that there will be negligible increase in the longitudinal bunch emittance, although the bunch shape will be distorted. However, when the initial normalized phase extent of the bunch $\hat{g}_i$ is less than $|\hat{g}_1|$, there will be an increase. The final normalized phase extent $\hat{g}_f$ is a complicated function of $\hat{g}_i$ and $\hat{g}_2$, and is illustrated in Table I and Fig. 3.

TABLE I. Final normalized phase extent of the bunch $\hat{g}_f$ when the initial normalized phase extent $\hat{g}_i < |\hat{g}_1|$ and the driving frequency is below bifurcation.

		$\hat{g}_f$
(a) $\hat{g}_2 > 0$	$\hat{g}_i < \hat{g}_2$	$< \lvert\hat{g}_1\rvert$
(b) $\hat{g}_2 > 0$	$\hat{g}_i > \hat{g}_2$	$\lvert\hat{g}_1\rvert$
(c) $\hat{g}_2 = 0$		$\lvert\hat{g}_1\rvert$
(d) $\hat{g}_2 < 0$	$\hat{g}_i > \lvert\hat{g}_2\rvert$	$\lvert\hat{g}_1\rvert$
(e) $\hat{g}_2 < 0$	$\hat{g}_i < \lvert\hat{g}_2\rvert$	$< \hat{g}_c$

Above bifurcation, there are no separatrices and therefore $\hat{g}_1$ cannot be defined. The only way to obtain the correct final phase extent of the bunch is to solve for the bunch trajectory. This can be accomplished by equating the Hamiltonian to its value at $\pm\hat{g}_i$ and solving for the relevant phase extent $\hat{g}$. Most of the time, these equations cannot be solved analytically. Thus, this method is not much different from numerical tracking. This applies to the situation of below bifurcation as well.

Sometimes the driving frequency has a large spread. From Fig. 3, it is evident

that the maximal emittance increase occurs when the initial normalized bunch extent $\hat{g}_i = |\hat{g}_2|$ ($\hat{g}_2 < 0$) and the final normalized bunch extent $\hat{g}_f = |\hat{g}_1|$. Therefore

$$\hat{g}_f = \hat{g}_c + \frac{2}{\sqrt{\hat{g}_c}} , \tag{6.1}$$

$$\hat{g}_i = \hat{g}_c - \frac{2}{\sqrt{\hat{g}_c}} . \tag{6.2}$$

We can define the fractional increase in amplitude as $f = (\hat{g}_f - \hat{g}_i)/\hat{g}_i$. This definition is very extreme, in the sense that the size of a bunch is measured by its extent rather than the rms of its particle distribution. Using Eqs. (6.1) and (6.2), we have

$$f = \frac{4}{\hat{g}_c^{3/2} - 2} . \tag{6.3}$$

Substituting back into Eq. (6.2), one obtains

$$\hat{g}_i = \frac{\frac{4}{f}}{\left(2 + \frac{4}{f}\right)^{1/3}} , \tag{6.4}$$

which gives the tolerance condition for a certain fractional emittance increase. For example, if the emittance increase has to be less than 50% (or amplitude increase $f < \sqrt{1.5} - 1 = 0.225$), one requires

$$\hat{g}_i = \frac{g_i}{(4a)^{1/3}} > 6.58 , \tag{6.5}$$

Or the driving amplitude must satisfy

$$a < \frac{1}{4}\left(\frac{g_i}{6.57}\right)^3 , \tag{6.6}$$

where g_i is the initial amplitude or initial phase extent of the bunch recovered from the *normalized* initial amplitude $\hat{g}_i$.

Sometimes given a driving amplitude a and an initial bunch phase extent g_i, one wants to compute the emittance increase. We can first construct the *normalized* initial amplitude $\hat{g}_i$. From Eq. (5.2) or

$$\hat{g}_c^{3/2} - \hat{g}_i \hat{g}_c^{1/2} - 2 = 0 \ , \tag{6.7}$$

$\hat{g}_c^{1/2}$ can be solved in terms of $\hat{g}_i$ in exactly the same way as given by Eq. (4.16). With Eq. (6.7), the fraction amplitude increase in Eq. (6.3) can also be written as

$$f = \frac{4}{\hat{g}_c^{1/2} \hat{g}_i} \ . \tag{6.8}$$

The final result is

$$f = \begin{cases} \dfrac{2\sqrt{3}}{\hat{g}_i^{3/2} \cosh \frac{\xi}{3}} & \hat{g}_i < 3 \\ \dfrac{2\sqrt{3}}{\hat{g}_i^{3/2} \cos \frac{\xi}{3}} & \hat{g}_i > 3 \end{cases} \tag{6.9}$$

where

$$\xi = \begin{cases} \tanh^{-1} \sqrt{1 - \left(\frac{\hat{g}_i}{3}\right)^3} & \hat{g}_i < 3 \\ \tan^{-1} \sqrt{\left(\frac{\hat{g}_i}{3}\right)^3 - 1} & \hat{g}_i > 3 \end{cases} \tag{6.10}$$

VII. GROUND MOTION AT SSC

In the collision mode at 20 TeV, the synchrotron frequency of the SSC collider rings is $\omega_{s0}/2\pi \sim 4.5$ Hz. However, ground vibrations usually have an appreciable intensity up to ~ 10 Hz. Therefore, ground motion may have an important impact on the longitudinal phase space.

A horizontal displacement of a quadrupole by Δ leads to an angular bending of the beam by $\hat{\theta} = \frac{\Delta}{f_q}$, f_q being the focal length of the quadrupole. The driving amplitude is therefore, according to Eq. (2.6),

$$a = \frac{hD\Delta}{\nu_{s0} C f_z} \ . \tag{7.1}$$

A quadrupole at the arc has length $\ell = 5.2$ m and field gradient $B' = 205$ T/m. The beam rigidity is $B\rho = 66712.8$ T-m, giving $f_q = 62.5$ m. The ring has a circumferential length of $C = 87.12$ km, rf harmonic $h = 104544$, and average dispersion $\langle D \rangle = 1.31$ m. The designed half bunch length is $\sqrt{6}\sigma = 0.175$ rf rad.

The two sources of ground motion which are of high intensity and sinusoidal structure are a quarry blast 9 miles away and a train crossing 20 m above the tunnel. There had been measurements [3] at tunnel depth. The horizontal ground motion for quarry blast can be summarized by *integrated* displacements over frequency of 0.143 μm near 1 Hz and 0.108μm near 3 Hz. The spectrum at 1 Hz is sharp, but that at 3 Hz is rather broad. The quarry blast, being far away, will affect all the 1600 quadrupoles randomly. The effect of the train crossing can also be described by horizontal *integrated* displacements of 0.055 μm near 3 Hz and 0.058μm near 7 Hz, and it affects only about 10 neighboring quadrupoles. Again the spectrum is rather broad.

For the quarry blast, we take the ground motion near 3 Hz and obtain a driving amplitude of $a = 9.34 \times 10^{-5}$. The normalized initial phase extent is $\hat{g}_i = 0.175/(4a)^{1/3} = 2.43$. Substituting into Eq. (6.9) gives an emittance increase of 253%. For the train crossing, we take the ground motion near 7 Hz and obtain a driving amplitude of $a = 1.19 \times 10^{-5}$, which gives an emittance increase of 82%. On the other hand, according to Eq. (6.6), the tolerance of 50% emittance increase is having a driving amplitude $a < 4.71 \times 10^{-6}$.

VIII. CURRENT RIPPLES

The power source always has a 60-cycle ripple that will perturb the dipole field. On the other hand, the synchrotron frequency f_{s0} of a machine may ramp through 60 Hz. The phase space may therefore be affected.

Unfortunately, Eqs. (6.6) and (6.9) cannot be used to compute the tolerance and fractional emittance increase, the reason being that the synchrotron frequency is increasing during the passage of 60 Hz. The emittance increase depends very critically on how fast the synchrotron frequency is changing and the initial positions of the bunch particles. If the synchrotron frequency changes *very* rapidly, the bunch particles will not be able to follow the island structure, and therefore the emittance increase will be minimal.

On the other extreme, the synchrotron frequency can change so slowly that the beam particles follow the islands exactly. When the synchrotron frequency is below the driving frequency, there is no island inside the rf bucket, and there is only one stable fixed point a which is close to the origin but on the right side. As the synchrotron frequency increases, this stable fixed point goes more negative and reaches $\hat{g}_a = -2$ at bifurcation frequency. The bunch or some of its particles will be oscillating around this fixed point and trapped inside this outer island. As synchrotron frequency increases further, this fixed point moves farther and farther away from the origin of the phase space and reaches the boundary of the rf bucket eventually. So the bunch will also reach the boundary of the rf bucket and beam loss will occur. The change of island structure will follow the sketches in Fig. 3 in the order of increasing $\hat{x}$ from [(a) to (e)]. A simulation of this situation was performed with a perturbation having a driving amplitude of $a = 0.01$ at a tune of $\nu_m = 0.01$. The synchrotron

tune was varied linearly from $\nu_{s0} = 0.005$ to 0.035 at a rate of $\Delta\nu_{s0} = 3.0 \times 10^{-9}$ per turn. Figure 4(a) shows the result of tracking a single particle in the normalized longitudinal phase space as a ν_m^{-1}-map. The particle started out at normalized phase $\hat{g}_i = 1.5$ and zero momentum offset. We see that the particle was trapped in the outer island and followed it to the boundary of the rf bucket.

In between these two extremes, the bunch emittance will usually be changed. A situation is shown in Fig. 4(b), where everything is the same as Fig. 4(a), with the only exception that the synchrotron tune was ramped much faster at the rate of $\Delta\nu_{s0} = 3.0 \times 10^{-7}$ per turn. It is obvious that the particle did not follow the outer island. It fell into the inner island oscillating around the stable fixed point b. In fact, the final normalized phase shrank to $\hat{g}_f \sim 0.5$. This does not mean that the bunch area decreases. The final normalized phase of a particle may become larger if it starts from a different $\hat{g}_i$.

Since $\nu_{s0} \propto \sqrt{|\eta|/E}$ from Eq. (2.3), we have

$$\frac{\Delta\nu_{s0}}{\nu_{s0}} = \frac{\Delta\eta}{2\eta} - \frac{\Delta\gamma}{2\gamma} = \frac{\dot{\gamma}\Delta t}{2\gamma}\left[\frac{2}{\eta\gamma^2} - 1\right] , \tag{8.1}$$

where γ is the Lorentz-transformation factor and Δt is the time for the synchrotron tune to change by $\Delta\nu_{s0}$. For RHIC, the synchroton frequency passes through 60 Hz when $\gamma = 17.5$ and $\dot{\gamma} = 1.6\ \mathrm{s}^{-1}$. The transition gamma is $\gamma_t = 23.6$. We have $\Delta\nu_{s0}/\nu_{s0} = -0.25\Delta t$, implying that f_{s0} changes by 12.5% in $\frac{1}{2}$ sec or in 30 synchrotron periods. The circumferential length of the RHIC ring is $C = 3833.84$. Thus ν_{s0} is changing at the rate of 2.45×10^{-9} per turn in the vicinity of $f_{s0} = 60$ Hz (or $\nu_{s0} = 7.67 \times 10^{-4}$).

Let ϵ be the fractional level of the 60 Hz ripples. This leads to a deflection of the beam by

$$\hat{\theta} = \frac{\hat{B}\ell}{B\rho} = 2\pi\epsilon \ , \tag{8.2}$$

for *all* the dipoles, where $\hat{B}$ is the peak value of the ripple magnetic field and ℓ is the *total* length of all the dipoles. The rf phase difference per turn is

$$\Delta\varphi = 2\pi\frac{\Delta C}{C} = \frac{4\pi^2 h D\epsilon}{C} = 3.52\epsilon \ , \tag{8.3}$$

where the rf harmonic $h = 342$ and the dispersion at the dipole $D \sim 1$ m have been used. The driving amplitude at synchrotron frequency $f_{s0} = 60$ Hz is

$$a = \frac{\Delta\varphi}{2\pi\nu_{s0}} = 731\epsilon \ . \tag{8.4}$$

The half bunch length at RHIC is expected to be 0.805 rf rad. Therefore, at ripple level $\epsilon = 10^{-6}$, the driving amplitude is $a = 7.31 \times 10^{-4}$ and the initial normalized phase extent of the bunch is $\hat{g}_i = 5.63$. A simulation was performed ramping from $\nu_{s0} = 1.0 \times 10^{-4}$ to 2.5×10^{-3}. The results show that particles from different parts of the bunch behaved differently. However, the normalized phase extent of the bunch increased only negligibly to $\hat{g}_f \sim 5.73$ or 4% for the emittance increase. If the ripple level becomes $\epsilon = 10^{-5}$, the emittance increase becomes 26%.

However, when the ripple level is as high as $\epsilon = 5 \times 10^{-5}$, the situation is completely different. We now have $a = 2.92 \times 10^{-2}$ and initial normalized phase extent of the bunch $\hat{g}_i = 1.52$. Similations show that particles having $\hat{g}_i$ less than 1.49 were trapped inside the outer island and were driven out to the boundary of the rf bucket. Therefore, to avoid appreciable emittance increase the ripple level must be well controlled and/or the ramping rate must be made faster.

Near the end of a ramping cycle, the synchrotron frequency will fall after the rf voltage has reached its maximum. There is also a possibility that the synchrotron

frequency will fall through a driving frequency. This change is usually slow. We can follow the sketches in Fig. 3 in the order of decreasing $\hat{x}$ [from (e) to (a)]. At first the extent of the separatrices is very big, so that the bunch is completely inside the inner island. As the synchrotron frequency decreases ($\hat{x}$ decreases), intercept 2 of the separatrices shrinks until it cuts into the left side of the bunch. Particles that have phases more negative than $\hat{g}_2$ will travel close to the separatrix reaching the other intercept 1. As the island structure continues to shrink as the synchrotron frequency decreases further, particles near intercept 1 will be left outside the island system. The increase will therefore be from $\hat{g}_i = |\hat{g}_1|$ to $\hat{g}_f = |\hat{g}_2|$, so that Eqs. (6.9) can be applied. However, one should remember that the island system is shrinking all the time. For example, particles leaving intercept 2 at some time will reach intercept 1 at a later time. Therefore, the actual increase should be less than that given by Eq. (6.9). As an illustration, a simulation having the same driving force of Fig. 4 was performed with synchrotron frequency decreasing from $\nu_{s0} = 0.035$ to 0.005 in steps of $\Delta\nu_{s0} = -3.0 \times 10^{-9}$ per turn. Figure 5(a) shows the tracking of a particle starting with normalized phase $\hat{g}_i = 1.5$. The final normalized phase was $\hat{g}_f = 3.2$, leading to a fractional phase increase of 1.1, whereas Eq. (6.9) gives 1.6. The ramping rate was next increased to $\Delta\nu_{s0} = -3.0 \times 10^{-7}$ per turn. Figure 5(b) shows that the final normalized phase was only $\hat{g}_f = 1.8$.

In our formulation of the theory in Sec. II, the driving amplitude a is defined in Eq. (2.6) with a factor of ν_{s0} for the sake of convenience. Since the driving amplitude is assumed to be time independent, this ν_{s0} in the perturbative part of the Hamiltonian of Eq. (2.7) should not be varied even when the synchrotron frequency is changing. Therefore, strictly speaking, our analysis cannot be applied here. However, we learn

from our simulations that the illustrations shown in Figs. 4 and 5 will not be changed by very much even if this precaution has been taken. Also the discussion in Sec. II is inside a *stationary* bucket. During the ramping of an accelerator, the bucket will be *moving* and smaller. However, our tracking results still hold qualitatively. For example, if the particle is trapped inside the outer island and moves with it to the boundary of the rf bucket as indicated in Fig. 4(a), this should happen in a moving bucket as well.

IX. CONCLUSION

We studied the particle motion in the longitudinal phase under the influence of the nonlinear rf force and a sinusoidal perturbation that has a driving frequency close to the synchrotron frequency. The phase space is divided up into resonant islands. The most important one is the first-order resonance, which had been analysed in detail. Beam particle motion will follow the trajectories inside the islands, which leads to an increase in the longitudinal emittance. This effect was applied to the ground motion perturbation on the quadrupoles of the SSC collider ring, when the frequency of the ground wave is close to the synchrotron frequency of the ring. We also discussed the effect of the 60 cycle current ripples in the dipoles of an accelerator ring, when the synchrotron frequency is ramped through 60 Hz. We discovered that the emittance increase depends very critically on the rate at which the synchrotron frequency is ramped and the initial size of the bunch. Although the more exact effects have to come from numerical simulations, however, the analytic treatment given in this paper will be found helpful in their interpretation.

REFERENCES

[1] K.Y. Ng, *Longitudinal Beam Motion due to Ground Motion*, Fermilab Internal Report FN-592, 1992.

[2] When $\hat{x} > 1$, the cubic is solved by using the identity $\cos\xi = 4\cos^3\frac{\xi}{3} - 3\cos\frac{\xi}{3}$ and letting $\hat{g} \propto \cos\frac{\xi}{3}$. When $\hat{x} < 1$, we let $\hat{g} \propto \cosh\frac{\xi}{3}$.

[3] K. Henon and D. Henon, Earth Technology Corporation, *Field Measurements and Analysis of Underground Vibrations at the SSC Site*, SSC Publication No. SSC-SR-1043, 1989.

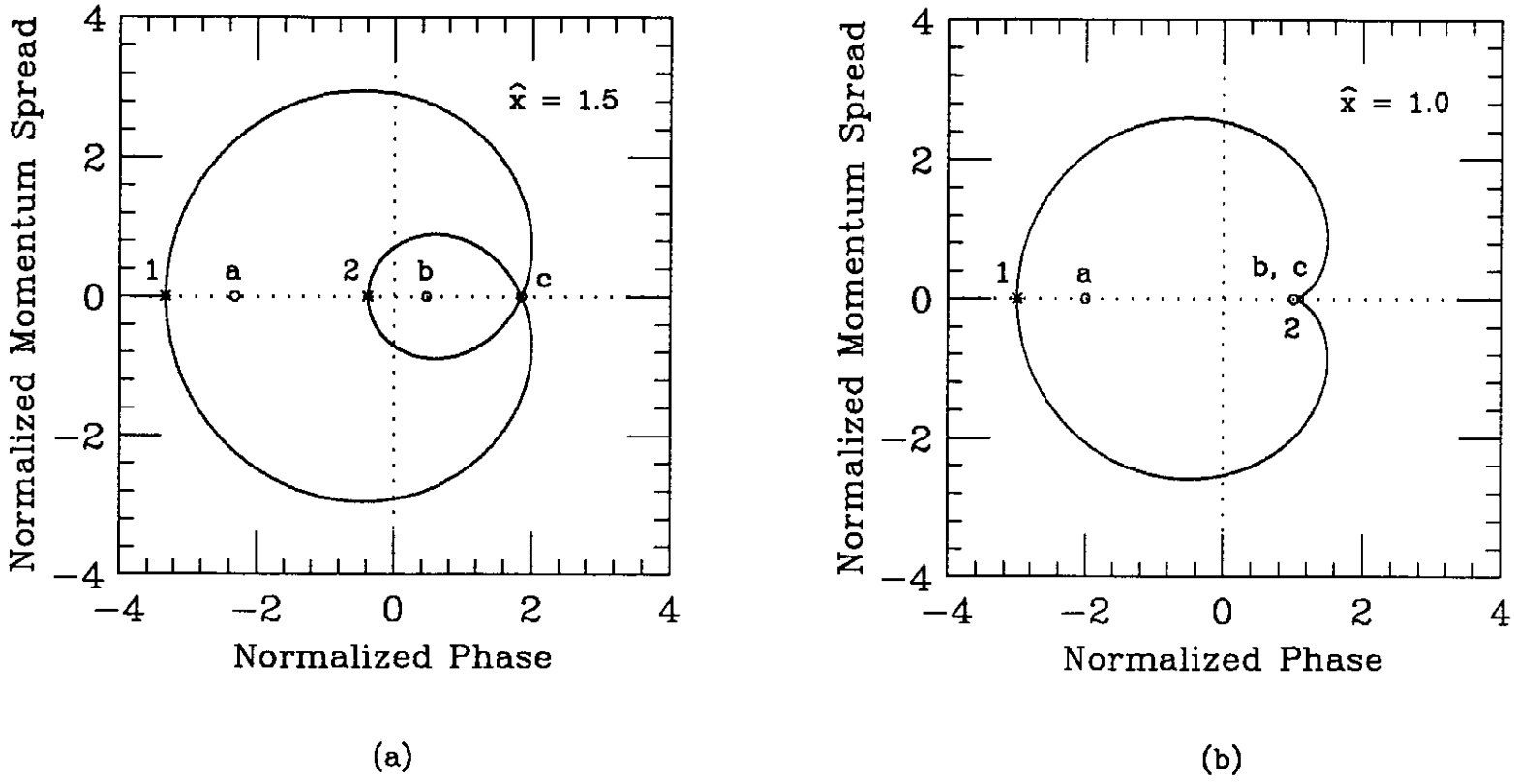

Figure 1: Fixed points and separatrices in the normalized longitudinal phase space when the driving frequency is (a) below bifurcation and (b) right at bifurcation.

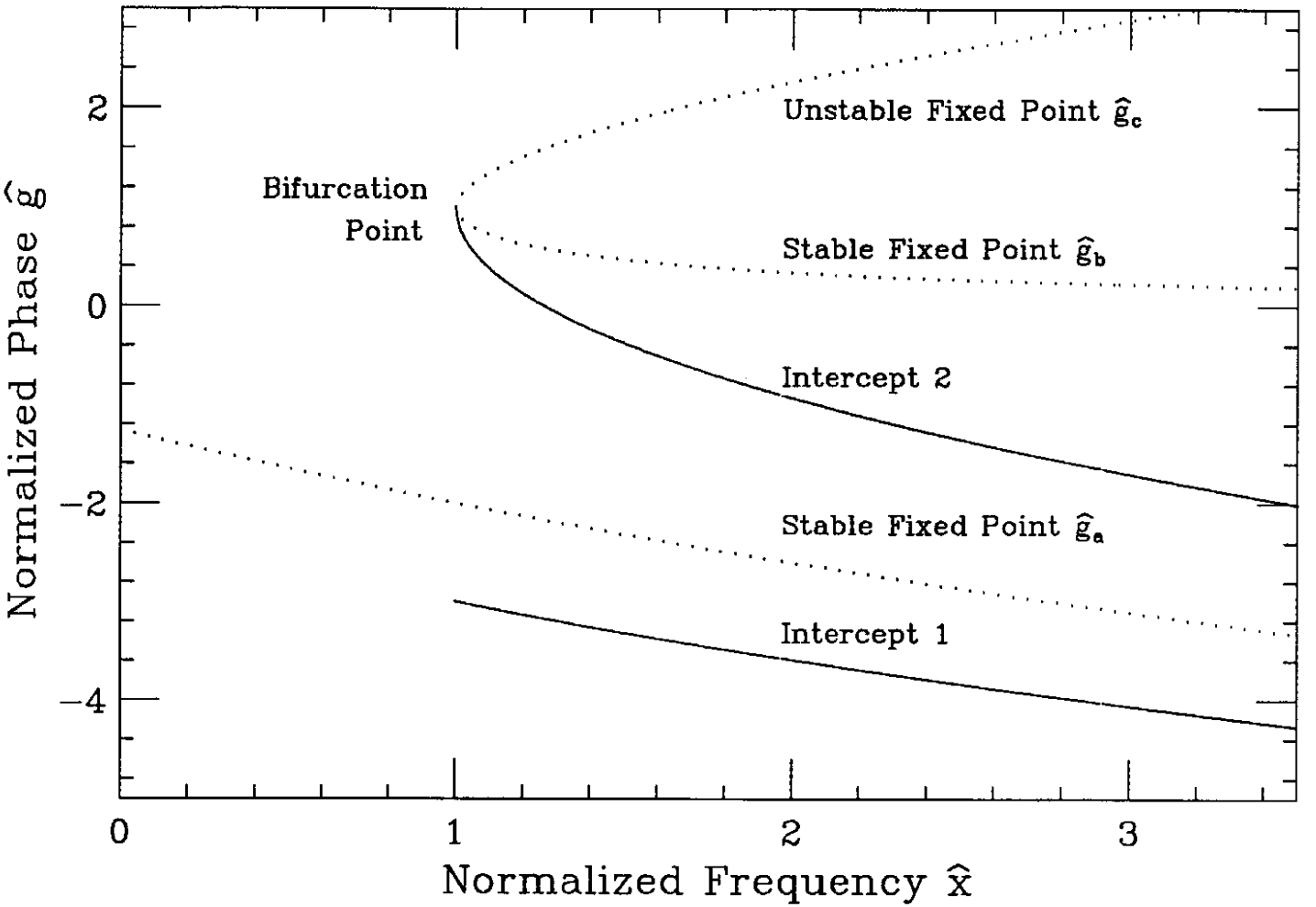

Figure 2: Stable, unstable fixed points, and separatrix intercepts vs normalized frequency.

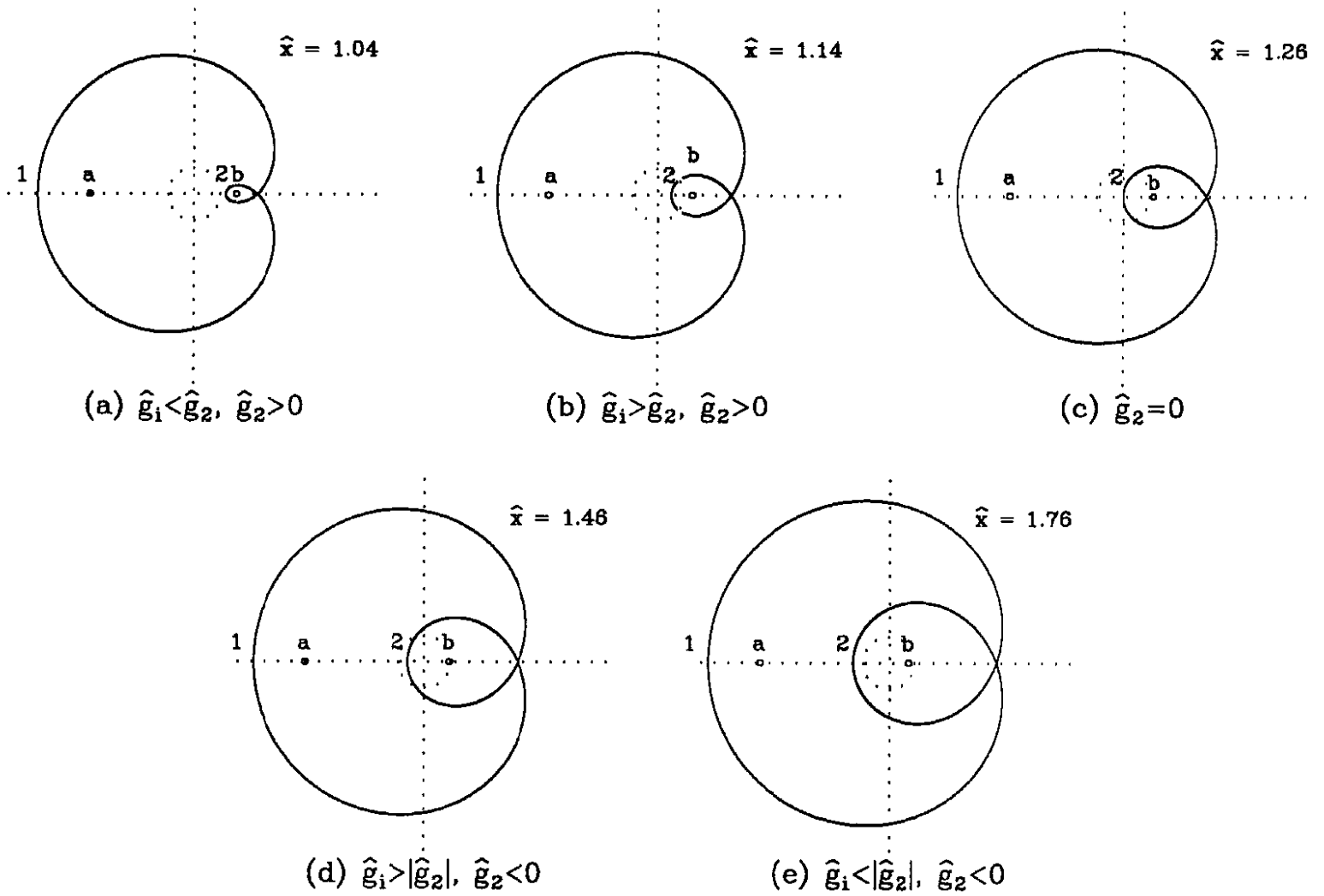

Figure 3: Illustration of emittance increase at 5 different driving frequencies below bifurcation as listed in Table I. The bunch is shown as a dotted circle.

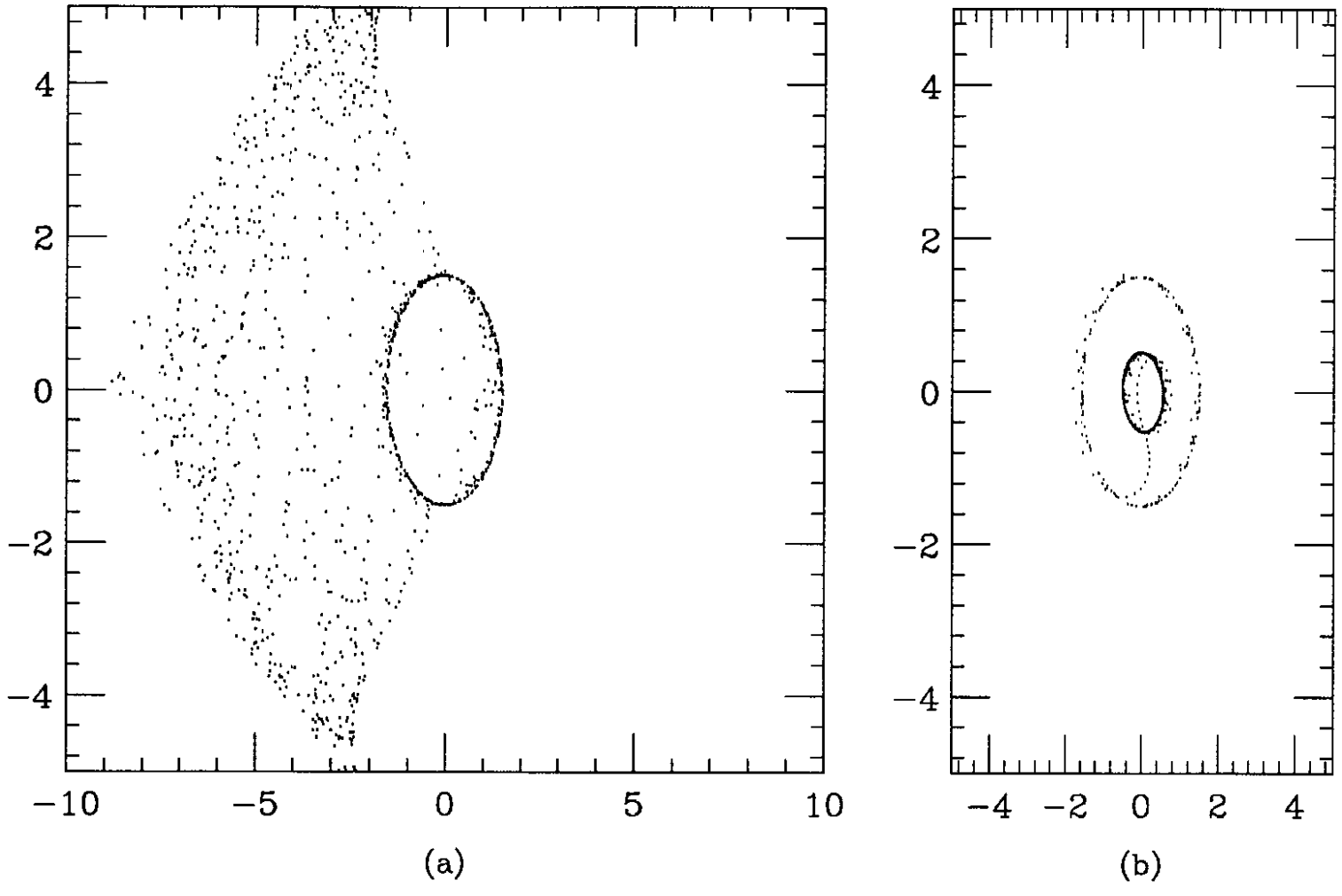

Figure 4: Tracking for a particle initially at normalized phase 1.5 from synchroton tune ν_{s0} = 0.005 to 0.035, changing at a rate of (a) $3.0\text{x}10^{-9}$ per turn and (b) $3.0\text{x}10^{-7}$ per turn. Driving amplitude is a = 0.01 at a tune of ν_m = 0.01.

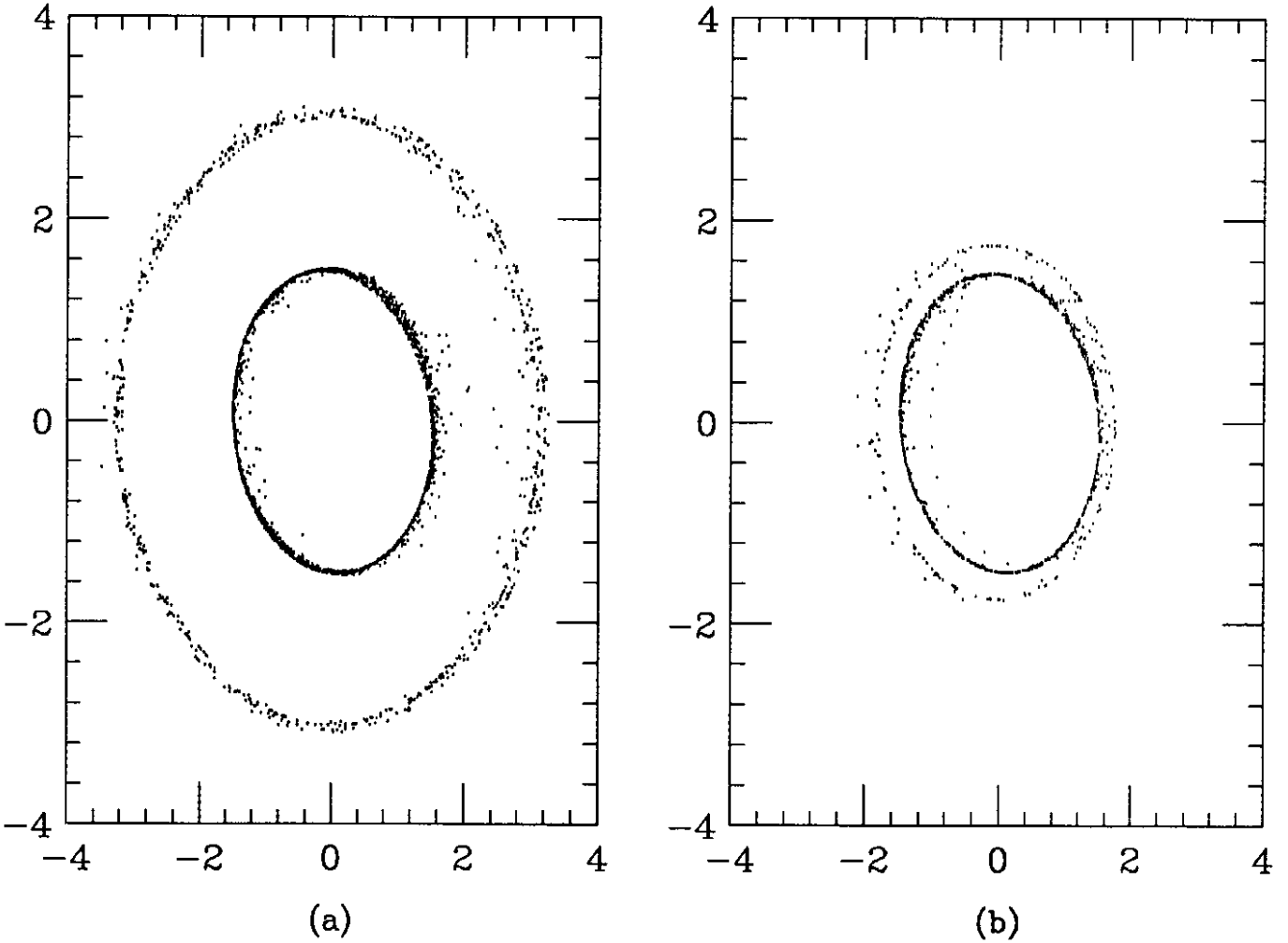

Figure 5: Tracking for a particle initially at normalized phase 1.5 from synchroton tune ν_{s0} = 0.355 to 0.005, changing at a rate of (a) $-3.0\text{x}10^{-9}$ per turn and (b) $-3.0\text{x}10^{-7}$ per turn. Driving amplitude is a = 0.01 at a tune of ν_m = 0.01.